Facile and versatile substrate fabrication for surface enhanced Raman spectroscopy using spark discharge generation of Au/Ag nanoparticles

Attila Kohut[a,b], Albert Kéri[b,c], Viktória Horváth[a,b], Judit Kopniczky[a,b], Tibor Ajtai[a,d], Béla Hopp[a,b], Gábor Galbács[b,c], Zsolt Geretovszky[a,b,*]

[a] Department of Optics and Quantum Electronics, University of Szeged, Dóm sq. 9, 6720 Szeged, Hungary
[b] Department of Materials Science, Interdisciplinary Excellence Centre, University of Szeged, 6720 Szeged, Dugonics sq. 13, Hungary
[c] Department of Inorganic and Analytical Chemistry, University of Szeged, Dóm sq. 7, 6720 Szeged, Hungary
[d] Department of Photonics and Laser, Interdisciplinary Excellence Centre, University of Szeged, 6720 Szeged, Dugonics sq. 13, Hungary

ABSTRACT

A simple, one-step gas phase technique for the fabrication of low-cost substrates with tunable plasmonic enhancement is proposed exploiting the unique peculiarities of spark discharge nanoparticle generation in particle mixing and the ease of particle deposition onto glass microfiber filters. The applicability of the spark-based technique to produce substrates for surface enhanced Raman measurements based on Au/Ag binary nanoparticles is discussed. Our results prove that considerable signal enhancement can be achieved over a large surface area, which can be conveniently tuned due to the inherent ability of the spark generator to mix two or more materials. This versatility in particle generation is well complemented by the direct deposition of the nanoparticles onto a filter medium, which makes the proposed method a low-cost and appealingly simple way for fabricating robust substrates for Raman-based applications.

1. Introduction

Surface enhanced Raman scattering (SERS) – first observed in 1974 [1] – is a well-known phenomenon employed in numerous analytical applications [2–6]. SERS-based methods effectively extend the non-destructive molecular recognition capabilities of Raman spectroscopy into the sub-ppb level [4], opening up the possibilities of single molecule sensing [7,8]. Since a suitable surface structure is needed for achieving significant and reliable signal enhancement, there is a continuous research interest towards the development of novel fabrication procedures and the improvement of the characteristics of SERS substrates [4]. These are typically either fabricated directly from a solid surface (e.g. by means of lithography), or employ metal nanoparticles (NPs) in a suspension or immobilized on a solid surface [9,10]. In the latter cases nanoparticles are usually synthesized by a wet chemical method [11–13], most commonly employing gold and silver and, to a lesser extent, copper, including their alloys or mixtures [9,14–19]. The size, shape and structure of NPs also play an important role in the SERS activity, for example core–shell Au/Ag structures are shown to exhibit higher enhancement than that of pure Au and Ag [16,17] and so are star- and triangle-shaped particles [9]. One reason for mixing gold and silver is the need for the symbiotic combination of the excellent

chemical stability of Au and the exceptionally high Raman signal enhancement of Ag [15]. In addition to this, varying the composition of Au/Ag alloys allows for the tuning of the plasmon band and hence the signal enhancement [15,20,21]. The latter can be especially important, since it has been shown that the optimum plasmon band, i.e. at which the enhancement is the largest, may vary with the specific molecule to be detected [15]. Therefore, tunability of the performance of a potential SERS material, e.g. via its elemental composition, is indispensable for the versatile fabrication of suitable substrates.

Wet chemical methods offer great potential for tuning the size, morphology and composition of NPs, but usually require various precursors, reagents, solvents, and often rather complicated and time-consuming sample preparation and synthesis routes [9]. These attributes affect the purity, stability and cost-effectiveness of the produced nanostructures, some aspects which are among the most important requirements of a good SERS substrate [4]. Physical NP generation processes and especially gas phase methods have the potential to eliminate many of the above shortcomings [22]. A technique which is standing out even among gas phase physical methods is the spark discharge nanoparticle generation. Spark discharge generators (SDG) – first introduced in 1988 [23] – employ repetitive, high current and high voltage, several microseconds long, oscillatory sparking between two

electrically conductive electrodes in a flowing gas [24–27]. Under these conditions the electrodes are eroded and their material is released into the gas phase, where – after nucleation, condensation and coagulation – NPs will form [28]. The method requires only bulk electrodes and a carrier gas – both available in high purity – so the purity of the particles can be well controlled and the process itself can be made environmentally friendly [29]. Moreover, the production can efficiently be scaled up due to the technical simplicity of the setup [30–32]. Another important feature of spark-based nanoparticle synthesis is the possibility of creating multielement NPs by using multielement (e.g. alloy, composite) and/or dissimilar electrodes [24,33–36]. Since spark based mixing occurs on the atomic level, multielement structures can be obtained even from materials immiscible in bulk form [37]. Spark-produced NPs have already shown their potential in various fields, including solar cell research [38,39], semiconductor science [40,41], environmental research [42,43], sensing [44–46], or in the textile industry [47]. Recently El-Aal *et al.* have reported that spark-produced silver nanoparticles – deposited on a copper substrate – exhibit excellent SERS-activity, indicating that SDG-grown NPs are ideal candidates for SERS applications [48]

In the present study we introduce a simple, one-step gas phase technique for the fabrication of low-cost substrates with tunable Raman signal enhancement by exploiting the advantages of spark discharge nanoparticle generation in elemental mixing and ease of aerosol phase NP deposition onto glass microfiber filters. The choice of this carrier is backed up by results of recent publications which demonstrate the usefulness of porous filters for the construction of inexpensive and easy-to-handle substrates for the detection of trace chemicals in either water [49,50] or air [51,52].

We generated Au/Ag binary nanoparticles (BNPs) with different compositions and deposited them onto glass microfiber filters. The morphology, size, and composition of the BNPs were characterized. The applicability of the SDG to produce SERS substrates as well as the potential in tuning the performance of the substrates by varying the Au/Ag composition are discussed.

2. Material and methods

2.1. Nanoparticle generation and deposition

The SDG setup used in the present experiments, schematically shown in Fig. 1, was formerly described in detail [53,54], hence we only give a brief overview below. It is based on a gas-tight stainless-steel chamber, housing a pair of cylindrical electrodes of 3.00 mm diameter, horizontally positioned and axially aligned inside the chamber. Au (99.9% purity, Goodfellow Cambridge Ltd.), Ag (99.9% purity, Goodfellow Cambridge Ltd.), and Au/Ag alloy (50/50 m/m%,

99.95% purity, ChemPUR GmbH.) electrodes were used in different combinations depending on the desired particle composition. The inter-electrode distance (i.e. the gap size) was controlled by micropositioners (K150-BLM-1, MDC Vacuum Ltd.) and set to 2.0 ± 0.1 mm for all results reported here. Argon (99.996% purity, Messer Hungarogáz Kft.) was employed as carrier gas, entering the chamber from below via an upward pointing inlet tube of 3 mm inner diameter, 5 mm away from the electrodes' common axis (referred to as upward pointing "cross-flow"). The gas flow rate was set to 5 L/min by a mass flow controller (GFC16, Aalborg Inc.). All experiments were carried out at atmospheric pressure, monitored by a piezo-resistive pressure gauge (VD81, Thyr-acont Vacuum Instruments GmbH.). A monolithic, high voltage, pulse discharge capacitor (450PM980, General Atomics Inc.) with a capacitance of 8 nF was connected parallel to the spark gap and charged by a high voltage capacitor charging power supply (HCK 800–12500, FuG GmbH.). The discharge of the capacitor between the electrodes commences when the capacitor voltage reaches the breakdown voltage. The resulting spark discharge is a bipolar, oscillatory discharge. The repetition rate of sparking was kept constant at 100 Hz by controlling the charging current of the capacitor. The voltage and current waveforms in the discharge loop were recorded by a digital storage oscilloscope (DSOX2024A, Keysight Technologies Inc.) using a high voltage probe (P6015A, Tektronix Inc.) and a current probe (110, Pearson Electronics Inc.), respectively.

The aerosol leaving the chamber passed through a tube furnace (EHA 12/300B, Carbolite Gero GmbH.), set to a constant temperature of 920 °C, performing the compaction of the nano-aggregates. The compacted NPs were collected on a 47 mm diameter glass microfiber filter (WHA1820047, Whatman plc), placed in a stainless-steel filter house (XX4404700, Millipore Corp.). The deposition time was controlled by an on/off valve before the filter house, and it was varied between 3 and 18 min.

2.2. Nanoparticle characterization

The size-distribution and the total concentration of the particles was measured by using a scanning mobility particle sizer, SMPS (consisting of a Model 3082 classifier and a Model 3756 particle counter, TSI Inc.). To this end a small, constant portion of the aerosol flow was diluted (VKL10, PALAS GmbH.) and directed into the SMPS. Morphology of the NPs was investigated by transmission electron microscopy (Tecnai G2 20 X-TWIN HR-TEM, Thermo Fisher Scientific Inc.), following sampling on grids (Lacey Carbon Films on 200 Mesh Copper Grids, Agar Scientific Ltd.) by means of a low-pressure impactor.

An inductively coupled plasma mass spectrometer (ICP-MS, 7700x, Agilent Technologies Inc.) was used for the determination of the composition of the NPs collected. Sample dissolution was carried out by
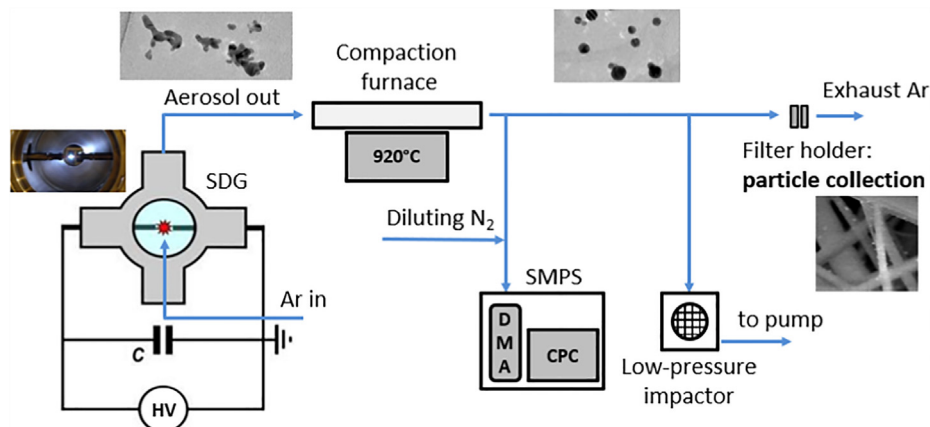

Fig. 1. The schematic view of the particle generation and characterization setup.

aqua regia, prepared freshly from trace quality cc. hydrochloric and cc. nitric acids (VWR Chemicals) under 16 h of contact time. The resulting clear solutions were filtered through 0.22 μm PTFE membrane filters and diluted with trace-quality de-ionized labwater (MilliPore Elix 10 equipped with a Synergy polishing unit, Merck GmbH.) prior to analysis. Multipoint, matrix-matched calibration was performed using certified calibration standards (IV-ICPMS-71A and IV-ICPMS-71C, Inorganic Ventures). ICP-MS plasma and interface parameters were optimized via standard tuning solutions (G1820-60410, Agilent). All measurements were carried out by monitoring the signal of the [107]Ag and [197]Au isotopes, in He mode using the ORS[3] collision cell. Data processing was performed within the Agilent Mass Hunter software. The 99.996% purity argon and 99.999% purity helium gases were purchased from Messer Hungarogáz Kft.

2.3. Raman spectroscopy

The performance of the substrates (i.e. the NP-loaded filters) was tested using 1 mM aqueous solutions of analytical purity Rhodamine 6G (R6G, Fluka AG) and Oxazine 1 (Oxa, Lambda Physik GmbH.). 10 μL test solution was dropped onto the substrate and left to dry on air for a few minutes. The Raman spectrum of the samples were measured using a fiber optic Raman spectrometer with diode laser excitation at 785 nm (laser: LASER-785-LAB-FC, spectrometer: QE65000, both Ocean Optics Inc.). 10 mW power and 1.0 s integration time were used for R6G, whereas 1 mW power and 0.5 s integration time for Oxa, without averaging. Each substrate was tested on at least five different spots, the average of which are reported below.

3. Results and discussion

3.1. Preparation and characterization of the substrates

As it was briefly mentioned in the Introduction, NPs of different materials can be flexibly made in an SDG by varying the electrodes between which the spark plasma is initiated. By using multielement (e.g. alloy, composite) and/or dissimilar elemental electrodes (e.g. Au and Ag), the generated BNPs will have a composition depending on the initial polarity of the electrodes and the characteristics of the oscillating spark discharge [33]. Here we use elemental gold and silver electrodes to generate Au/Ag BNPs for the fabrication of SERS substrates. Fig. 2A illustrates the typical morphology of the particles generated in the present experiments. It should be noted that our SDG setup uses a tube furnace to heat up the generated aerosol and therefore compact the as formed NP aggregates. The resulting particles have nearly perfect spherical shape (see the inset of Fig. 2A) and their size follows a log-normal distribution with a modal diameter of around 10 nm, as shown in the size distribution in Fig. 2C. The EDX analysis of the particles confirms the presence of both Au and Ag[1] (Fig. 2B), indicating the formation of Au/Ag alloys as expected under the present conditions [55].

The average elemental composition of the generated BNPs was determined by means of ICP-MS analysis, which resulted in 23.1 ± 1.0 m/m% Ag content. The lower concentration of Ag compared to Au is due to the different erosion rates of the two materials [27]. Under the same conditions, Au erodes approx. two to three times faster than Ag, which qualitatively explains the obtained Au/Ag composition.

In order to demonstrate the applicability of the SDG technique in the facile fabrication of simple and robust SERS substrates, the produced Au/Ag BNPs were collected on a glass microfiber filter placed downstream of the SDG. The deposition time was arbitrarily set to a few

minutes, until the presence of particles was visibly discernible over the surface of the filter. These particle-loaded filters were used as SERS substrates without any further conditioning and their performance was tested via measuring the Raman spectrum of R6G analyte (see the Material and methods section).

Fig. 3 shows the Raman spectrum of the R6G analyte measured on a bare glass microfiber filter and on the substrate containing SDG-produced Au/Ag BNPs. The enhancement of the Raman signal is obvious in case of the prepared substrates, since none of the R6G peaks are discernible on the bare filter. This clearly confirms the SERS effect of the substrates fabricated in only a few minutes. The average enhancement factor[2] corresponding to our substrates was found to be in the order of 10^4, which is close to typical values reported for other filter-based SERS substrates [49,51]. It is worth noting that the deposition process applied here allows for varying the active area of the substrate conveniently. In the present experiments, even at a deposition as short as a few minutes, the particles were distributed over a ca. 20 mm diameter area. Enhancement of the Raman signal of the probe analyte was confirmed all over the substrate surface, exhibiting a relative standard deviation of about 27%. Please note that the repeatability of the measured intensity depends on the deposition time and can be significantly increased as will be shown later in Fig. 7. It should also be added that spark discharge NP generation is proven to be scalable. The particle yield can effectively be upscaled by either increasing the spark repetition rate [30] or parallelization of SDG units [32]. Due to the relative simplicity of the set-up and low demand for precursor materials, the SDG is considered to be a cost-effective NP generator [24]. In the present case the electrical energy consumed by all the equipment of the generator setup during the preparation of one sample was about 0.1 kWh. In addition to this, by taking into account the price of one glass microfiber filter, and the amount of carrier gas (~50 L) and electrode material (a few tens of μg of gold and silver) consumed, the cost of manufacturing a single SERS substrate – without labor costs – is about 1 EUR.

3.2. Tuning of the substrates

It was shown in the previous subchapter that Au/Ag BNPs can be simply and effectively produced in an SDG to fabricate efficient SERS substrates from glass microfiber filters. The inherent properties of the spark-based technique (e.g. mixing) not only allows for the generation of SERS active substrates, but also offer possibility for tuning the performance of the produced substrates by varying the composition of the generated BNPs. There are two distinctly different strategies to produce BNPs in an SDG. The first one, which was used above, relies on the application of two dissimilar elemental electrodes (here Au and Ag), while the second method uses electrodes made by alloying or sintering two or more elements together (e.g. Au and Ag), the initial composition of which will be preserved in the generated BNPs [34,55]. In the present study, we combine these two strategies in order to widen the range, in which the composition of the generated NPs can be tuned. Three pairs of electrodes (pure Au, pure Ag and an Au/Ag alloy with a 50 m/m% nominal Ag concentration) were used in different combinations to produce NPs in six different compositions. The electrode configurations tested and the resulting average elemental composition of the generated NPs, determined by ICP-MS analysis, are summarized in Table 1.

As shown in Table 1, with the combination of only three electrodes in six geometries the entire composition range can neatly be covered in a fairly uniform manner. The slight shift towards higher Au content is due to the higher electrode erosion rates of Au with respect to Ag, as

---

[1] Please note that the peaks assigned to Cu in the EDX spectrum originate from the material of the TEM grid.

[2] The enhancement factor of the substrates was calculated by comparing the intensity of surface-enhanced and regular Raman spectra of analytes of lower and higher concentrations, respectively, measured with and without nanostructures, according to the widely used formula detailed in e.g. [49].
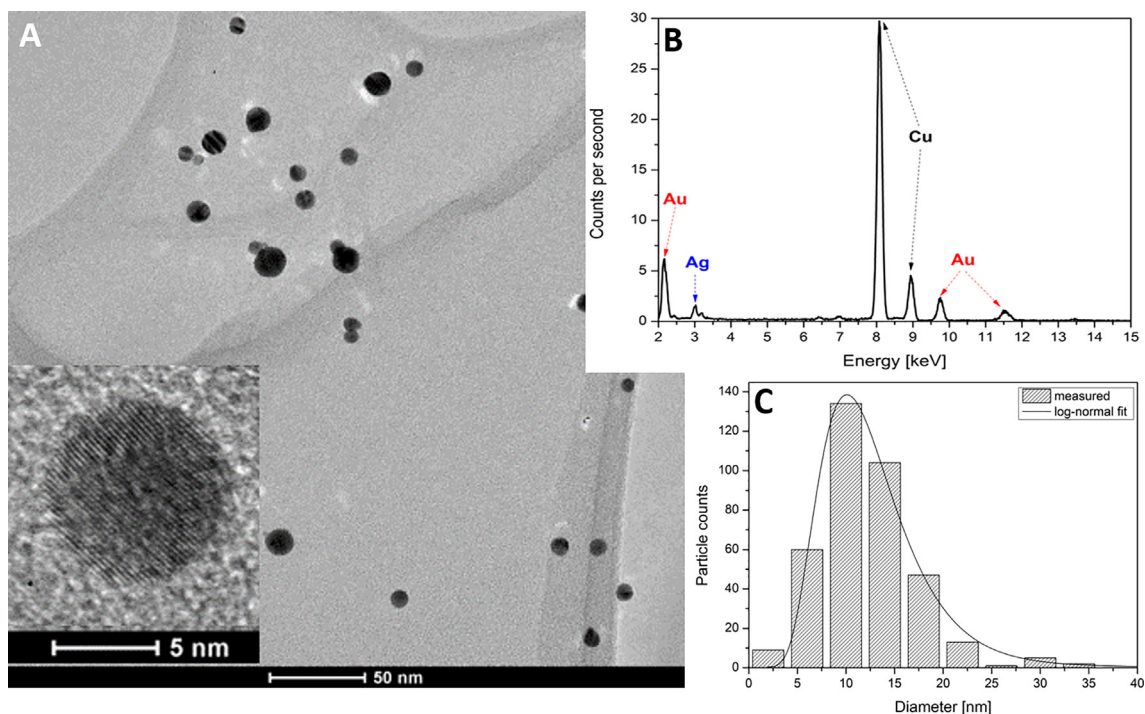
Fig. 2. Structural and compositional properties of Au/Ag BNPs generated using initially anodic gold and initially cathodic silver electrodes and post-compacted at 920 °C. (A) TEM micrograph of compacted Au/Ag BNPs, along with a HR-TEM of a single particle in the inset. EDX spectrum (B) and size distribution (C) of the generated BNP population.
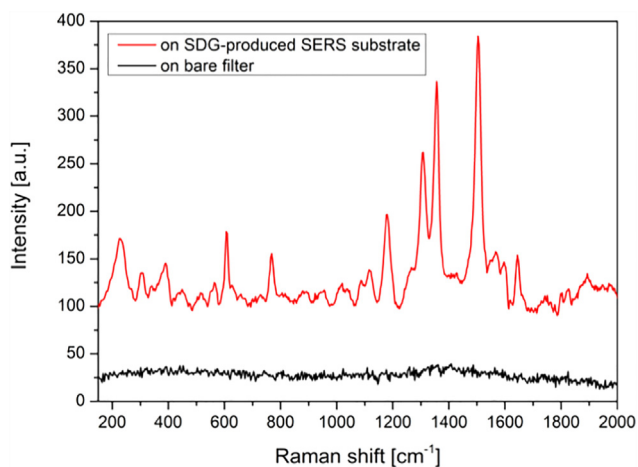

Fig. 3. Raman spectra of R6G measured at 785 nm excitation on a bare filter (black) and on a filter loaded with Au/Ag BNPs generated by using initially anodic gold and cathodic silver electrodes (red). The red spectrum is vertically shifted for better visibility. (For interpretation of the references to color in this figure legend, the reader is referred to the web version of this article.)

mentioned earlier. It should be noted that this effect is also reflected in the number concentration of the generated particles: the highest number concentration is obtained for pure Au, while the lowest is for pure Ag NPs with intermediate values for each BNP composition. In order to keep the particle density constant on the surface of the filters, this effect was compensated: we adjusted the particle deposition time in accordance with the variation of the NP number concentration obtained at constant sampling time. As a result, filters loaded with pure Au had the shortest (ca. 3 min), while Ag-loaded ones had the longest (ca. 18 min) deposition time.

The variation of the surface plasmon resonance (SPR) band as a function of Au/Ag composition of NPs deposited on the filter is shown in Fig. 4. The blue-shifting of the SPR with increasing silver content is

Table 1

Electrode configurations used and the average elemental composition of the SDG-produced NPs. Measurement errors are shown as confidence intervals at the 90% level and calculated from three independent measurements.

Nominal composition and initial polarity of the electrodes		Average measured concentration of Ag in the generated NPs [m/m%]
Anode	Cathode	
Au 100	Au 100	0*
Ag 100	Au 100	17.7 ± 0.2
Au 100	Ag 100	23.1 ± 1.0
Au 50/Ag 50	Au 50/Ag 50	44.6 ± 5.0
Ag 100	Au 50/Ag 50	67.5 ± 4.4
Ag 100	Ag 100	100*

* Nominal value.

clearly discernible. Moreover, as shown in the inset of Fig. 4, the shift of peak positions neatly follows the theoretical trend calculated by using the Mie theory[3], where single Au/Ag BNPs with a size distribution shown in Fig. 2C were considered. The good agreement between the experimentally obtained values and the calculated trend indicates that the measured average Au/Ag compositions well describe the substrates and there is no significant aggregation of the NPs.

The effect of NP composition on the performance of SERS substrates was tested for both analytes, namely Rhodamine 6G and Oxazyne 1 (see the Material and methods). At the experimental conditions used here, the Raman spectra of both solutions were unmeasurable on bare filters. It is apparent from Fig. 5 that the intensity of the characteristic Raman peaks, and hence the enhancement of the spectra varies differently with the particle composition for the two analytes. Pure Ag particles provide the highest enhancement for R6G (Fig. 5A), and the lowest for Oxa (Fig. 5B). For Oxa, the optimal BNP composition was found to be

---

[3] We used the MiePlot computer program, available at www.philipla-ven.com/mieplot.htm, for these calculations.
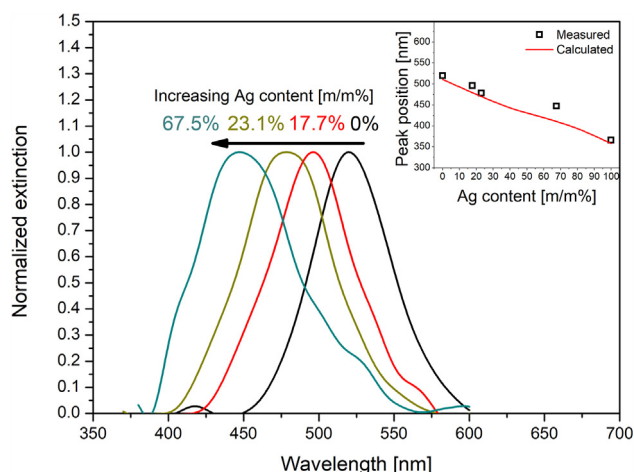
Fig. 4. SPR band of spark generated Au/Ag nanoparticles, deposited on glass microfiber filters, as a function of NP composition. The inset compares the measured peak positions to the trend calculated according to the Mie theory. All spectra are corrected for the baseline and normalized. Measured spectra were smoothed with a 25 pts FFT filter during processing.
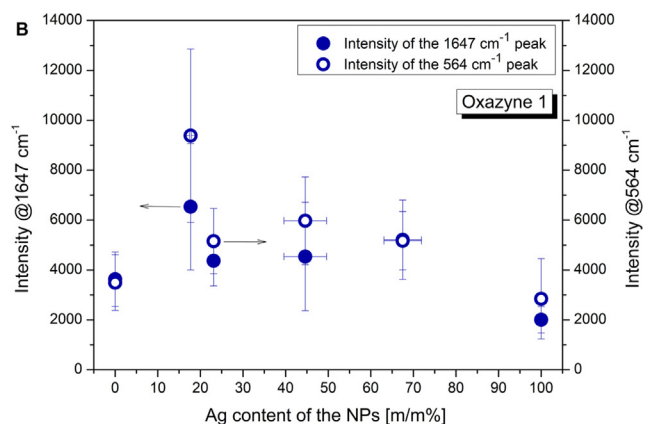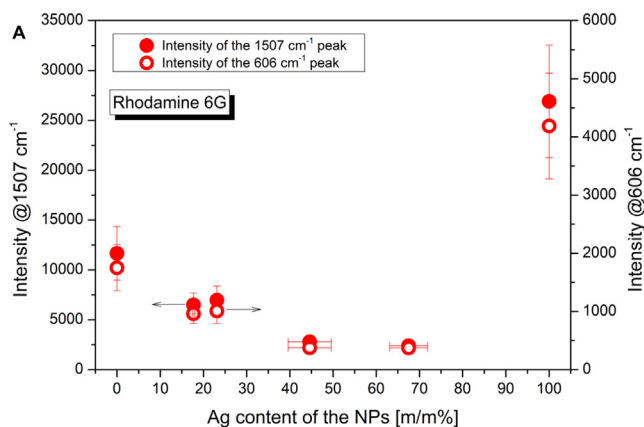

Fig. 5. Intensity variation of two characteristic Raman lines of R6G (A) and Oxa (B) as a function of particle composition, measured at 785 nm excitation. Standard deviation of the intensity measured at randomly selected spots over a substrate are shown as vertical error bars and the confidence intervals of the particle compositions at the 90% level are shown as horizontal error bars.

also showing the micrograph of a clean filter for reference. It can be qualitatively seen that the particles are uniformly distributed over the surface, there are no obvious discontinuities in the particle coverage. This is further strengthened when looking at a close-up of the substrate (cf. top right optical micrograph). The Au NPs (with which this particular substrate was made) fairly evenly cover the filter, indicated by the reddish tint of the substrate with respect to the greyish-white color of the empty filter shown in the top left corner. The NPs also uniformly cover each and every fiber, without significant aggregation, as can be seen in the SEM micrograph (bottom right panel). These observations visually support the good agreement between the measured and calculated SPR peaks shown in the inset of Fig. 4.

The effect of deposition time on the Raman intensity measured over the substrates is shown in Fig. 7. The Raman intensity of the 1507 cm^{-1} R6G peak is increasing linearly with increasing deposition time up to the longest deposition time (35 mins) studied here. Approx. 75% higher SERS signal can be obtained by increasing the deposition time by a factor of 5. An added benefit of higher NP surface coverage is the concomitant decreases of relative standard deviation across the sample by about 50%. In case of the substrate shown in Figs. 6 and 7, this results in a relative standard deviation of only about 17%. These SERS signal repeatability values favorably compare to the values reported in
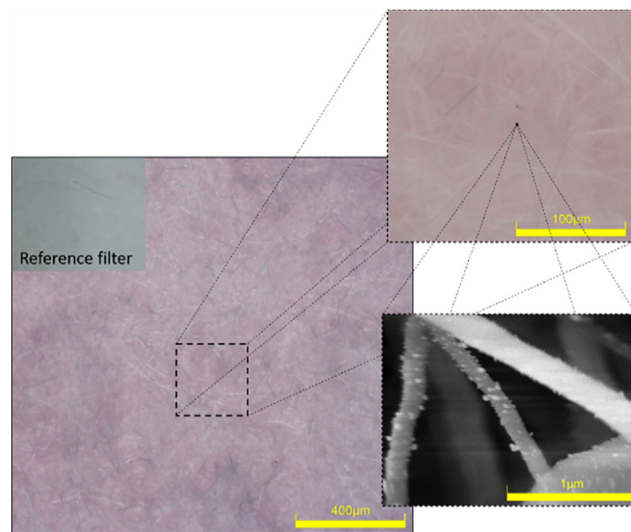
around 18 m/m% Ag content, while every alloy BNP exhibited higher enhancement than that of pure Au and Ag NPs (Fig. 5B). Similar results, namely that different Au/Ag compositions are optimal for achieving maximum enhancement of different analytes, were obtained by Fan *et al.*, which was explained by the selective binding of the molecules to different metallic domains on the BNPs [15]. This behavior provides solid ground that tuning the enhancement spectrum of a SERS substrate is a must, which can be conveniently achieved in SDGs via tuning the composition of the generated NPs. Apart from the enhancement-optimization, bimetallic SERS substrates can also be appealing over monometallic substrates, especially pure Ag NPs in many applications, due to the increased chemical stability of BNPs, originating from the incorporation of exceptionally stable Au [15].

It was demonstrated above that the ability of the spark discharge NP generation technique in producing Au/Ag BNPs with variable composition can be effectively utilized to fabricate and tune the performance of SERS substrates. However, in addition to changing the elemental composition of particles, other possibilities also exist to optimize the substrate performance. The variation of the deposition time offers the most straightforward way to affect the performance of the substrate. This practically determines the quantity of the deposited nanomaterial and hence varies the coverage of NPs over the surface.

The largest panel of Fig. 6 is an overview image of the substrate,

Fig. 6. Optical and scanning electron micrographs of a substrate with successively increasing magnification. Optical micrograph of a clean filter is shown in the inset as reference. The substrates are fabricated from gold NPs with a deposition time of about 3 min (the shortest time used in the experiments).
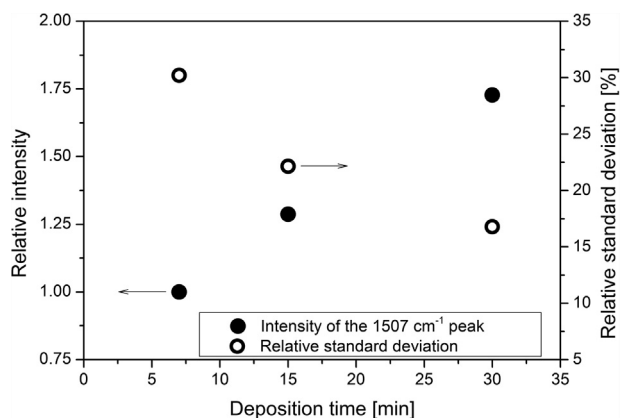
Fig. 7. Change of relative intensity (full black circles) and relative standard deviation of the intensity (empty black circles) of a characteristic R6G peak as a function of particle deposition time (surface NP coverage). Data presented refer to substrates loaded with elemental Au NPs.

the literature for other filter-based SERS substrates, ranging between 12 and 22% [56], or e.g. 20–25% [57,58]. Hence at longer depositions not only the SERS signal can be increased but the uniformity of the sample also improves. It should be noted that the trends shown in Fig. 7 are expected to be maintained only until aggregation of particles is insignificant on the surface. Beyond that, enhancement should increase in expense of surface uniformity [4].

4. Conclusions

Spark discharge nanoparticle generation was employed to fabricate SERS-active substrates by depositing silver/gold binary nanoparticles of varying composition from the gas phase on glass microfiber filters. The SERS performance of the as-formed substrates have been tested by using aqueous solutions of Rhodamine 6G and Oxazine 1. It was shown that the produced nanoparticles provide signal enhancement and that the signal enhancement can be tuned by changing the Au/Ag composition of NPs. It was found that in case of Rhodamine 6G, the strongest enhancement can be achieved using pure Ag particles, while BNPs with about 18% Ag content provided the highest signal for measuring Oxazine 1. Our results prove that the spark discharge nanoparticle generation technique provides a facile, cost-effective, yet robust and versatile way for producing substrates for surface enhanced Raman spectroscopy. The gas phase nature of the generation process allows for the direct deposition of the nanoparticles onto a filter medium, an appealingly simple fabrication method. Moreover, the inherent ability of the SDG to mix two or more materials by simply using different electrodes provides a very convenient way for tuning the composition of the generated particles, and hence the SERS-performance of the substrate. The need for such tunability was clearly demonstrated by the fact that different particle compositions were found to be optimal for the detection of two different test analytes. All the above features make the spark-based generation technique a good candidate for the production of substrates with plasmonic enhancement.

CRediT authorship contribution statement

Attila Kohut: Conceptualization, Methodology, Writing - original draft. **Albert Kéri:** Methodology, Investigation. **Viktória Horváth:** Investigation. **Judit Kopniczky:** Investigation, Visualization. **Tibor Ajtai:** Investigation, Data curation. **Béla Hopp:** Funding acquisition, Project administration. **Gábor Galbács:** Supervision, Writing - review & editing. **Zsolt Geretovszky:** Supervision, Validation, Writing - review & editing.

Declaration of Competing Interest

The authors declare that they have no known competing financial interests or personal relationships that could have appeared to influence the work reported in this paper.

References

[1] M. Fleischmann, P.J. Hendra, A.J. McQuillan, Chem. Phys. Lett. 26 (1974) 163.
[2] X. Qian, X.H. Peng, D.O. Ansari, Q. Yin-Goen, G.Z. Chen, D.M. Shin, L. Yang, A.N. Young, M.D. Wang, S. Nie, Nat. Biotechnol. 26 (2008) 83.
[3] M.E. Stewart, C.R. Anderton, L.B. Thompson, J. Maria, S.K. Gray, J.A. Rogers, R.G. Nuzzo, Chem. Rev. 108 (2008) 494.
[4] R. Pilot, R. Signorini, C. Durante, L. Orian, M. Bhamidipati, L. Fabris, Biosensors 9 (2019) 57.
[5] J.F. Li, Y.F. Huang, Y. Ding, Z.L. Yang, S.B. Li, X.S. Zhou, F.R. Fan, W. Zhang, Z.Y. Zhou, D.Y. Wu, B. Ren, Z.L. Wang, Z.Q. Tian, Nature 464 (2010) 392.
[6] I.A. Larmour, K. Faulds, D. Graham, Chem. Sci. 1 (2010) 151.
[7] K. Kneipp, Y. Wang, H. Kneipp, L.T. Perelman, I. Itzkan, R.R. Dasari, M.S. Feld, Phys. Rev. Lett. 78 (1997) 1667.
[8] P.G. Etchegoin, E.C. Le Ru, Phys. Chem. Chem. Phys. 10 (2008) 6079.
[9] P. Mosier-Boss, Nanomaterials 7 (2017) 142.
[10] D. Huang, Z. Zhuang, Z. Wang, S. Li, H. Zhong, Z. Liu, Z. Guo, W. Zhang, Appl. Surf. Sci. 497 (2019) 143825.
[11] P.C. Lee, D. Meisel, J. Phys. Chem. 86 (1982) 3391.
[12] R.J.C. Brown, M.J.T. Milton, J. Raman Spectrosc. 39 (2008) 1313.
[13] M.R. Jones, K.D. Osberg, R.J. Macfarlane, M.R. Langille, C.A. Mirkin, Chem. Rev. 111 (2011) 3736.
[14] Y. Fleger, M. Rosenbluh, Res. Lett. Opt. 2009 (2009) 1.
[15] M. Fan, F.J. Lai, H.L. Chou, W.T. Lu, B.J. Hwang, A.G. Brolo, Chem. Sci. 4 (2013) 509.
[16] L. Feng, G. Gao, P. Huang, K. Wang, X. Wang, T. Luo, C. Zhang, Nano Biomed. Eng. 2 (2011) 258–267.
[17] Y. Yang, J. Shi, G. Kawamura, M. Nogami, Scr. Mater. 58 (2008) 862.
[18] D.G. Gromov, S.V. Dubkov, A.I. Savitskiy, Y.P. Shaman, A.A. Polokhin, I.A. Belogorokhov, A.Y. Trifonov, Appl. Surf. Sci. 489 (2019) 701.
[19] P. Fu, X. Shi, F. Jiang, X. Xu, Appl. Surf. Sci. 501 (2020) 144269.
[20] O. Olea-Mejía, M. Fernández-Mondragón, G. Rodríguez-De La Concha, M. Camacho-López, Appl. Surf. Sci. 348 (2015) 66.
[21] Y. Sun, Y. Xia, Analyst 128 (2003) 686.
[22] G. Biskos, V. Vons, C.U. Yurteri, A. Schmidt-Ott, KONA Powder Part. J. 26 (2008) 13.
[23] S. Schwyn, E. Garwin, A. Schmidt-Ott, J. Aerosol Sci. 19 (1988) 639.
[24] T.V. Pfeiffer, J. Feng, A. Schmidt-Ott, Adv. Powder Technol. 25 (2014) 56.
[25] A. Kohut, L. Ludvigsson, B.O. Meuller, K. Deppert, M.E. Messing, G. Galbács, Z. Geretovszky, Nanotechnology 28 (2017) 475603.
[26] B.O. Meuller, M.E. Messing, D.L.J. Engberg, A.M. Jansson, L.I.M. Johansson, S.M. Norlén, N. Tureson, K. Deppert, Aerosol Sci. Technol. 46 (2012) 1256.
[27] N.S. Tabrizi, M. Ullmann, V.A. Vons, U. Lafont, A. Schmidt-Ott, J. Nanoparticle Res. 11 (2009) 315.
[28] J. Feng, L. Huang, L. Ludvigsson, M.E. Messing, A. Maisser, G. Biskos, A. Schmidt-Ott, J. Phys. Chem. C 120 (2016) 621.
[29] J. Feng, X. Guo, N. Ramlawi, T.V. Pfeiffer, R. Geutjens, S. Basak, H. Nirschl, G. Biskos, H.W. Zandbergen, A. Schmidt-Ott, J. Mater. Chem. A 4 (2016) 11222.
[30] J. Feng, G. Biskos, A. Schmidt-Ott, Sci. Rep. 5 (2015) 15788.
[31] M. Slotte, R. Zevenhoven, Energies 10 (2017) 1605.
[32] http://www.buonapart-e.eu/ (accessed: 19th of July 2020).
[33] J. Feng, N. Ramlawi, G. Biskos, A. Schmidt-Ott, Aerosol Sci. Technol. 52 (2018) 505.
[34] J. Feng, R. Geutjens, N.V. Thang, J. Li, X. Guo, A. Kéri, S. Basak, G. Galbács, G. Biskos, H. Nirschl, H.W. Zandbergen, E. Brück, A. Schmidt-Ott, A.C.S. Appl, Mater. Interfaces 10 (2018) 6073.
[35] A. Muntean, M. Wagner, J. Meyer, M. Seipenbusch, J. Nanoparticle Res. 18 (2016) 229.
[36] N.S. Tabrizi, Q. Xu, N.M. Van Der Pers, U. Lafont, A. Schmidt-Ott, J. Nanoparticle Res. 11 (2009) 1209.

[37] N.S. Tabrizi, Q. Xu, N.M. Van Der Pers, A. Schmidt-Ott, J. Nanoparticle Res. 12 (2010) 247.
[38] S. Jang, J. Yoon, K. Ha, M.-C. Kim, D.H. Kim, S.M. Kim, S.M. Kang, S.J. Park, H.S. Jung, M. Choi, Nano Energy 22 (2016) 499.
[39] T.V. Pfeiffer, J. Ortiz-Gonzalez, R. Santbergen, H. Tan, A. Schmidt Ott, M. Zeman, A.H.M. Smets, Energy Procedia 60 (2014) 3.
[40] M.H. Magnusson, B.J. Ohlsson, M.T. Björk, K.A. Dick, M.T. Borgström, K. Deppert, L. Samuelson, Front. Phys. 9 (2014) 398.
[41] M.E. Messing, K. Hillerich, J. Bolinsson, K. Storm, J. Johansson, K.A. Dick, K. Deppert, Nano Res. 3 (2010) 506.
[42] C. Helsper, W. Mölter, F. Löffler, C. Wadenpohl, S. Kaufmann, G. Wenninger, W. Molter, F. Loffler, C. Wadenpohl, S. Kaufmann, G. Wenninger, Atmos. Environ. Part A, Gen. Top. 27 (1993) 1271.
[43] C. Roth, G.A. Ferron, E. Karg, B. Lentner, G. Schumann, S. Takenaka, J. Heyder, Aerosol Sci. Technol. 38 (2004) 228.
[44] N.A. Isaac, P. Ngene, R.J. Westerwaal, J. Gaury, B. Dam, A. Schmidt-Ott, G. Biskos, Sensors Actuators B Chem. 221 (2015) 290.
[45] N.A. Isaac, M. Valenti, A. Schmidt-Ott, G. Biskos, ACS Appl. Mater. Interfaces 8 (2016) 3933.
[46] A.A. Efimov, I.A. Volkov, V.V. Ivanov, A.A. Vasiliev, A.E. Varfolomeev, A.V. Pislyakov, A.S. Lagutin, T. Maeder, Procedia Eng. 168 (2016) 1036.
[47] J. Feng, E. Hontañón, M. Blanes, J. Meyer, X. Guo, L. Santos, L. Paltrinieri, N. Ramlawi, L.C.P.M. de Smet, H. Nirschl, F.E. Kruis, A. Schmidt-Ott, G. Biskos, A.C.S. Appl. Mater. Interfaces 8 (2016) 14756.
[48] M.A. El-Aal, T. Seto, M. Kumita, A.A. Abdelaziz, Y. Otani, Opt. Mater. (Amst). 83 (2018) 263.
[49] W.W. Yu, I.M. White, Analyst 137 (2012) 1168.
[50] S. Fateixa, M. Raposo, H.I.S. Nogueira, T. Trindade, Talanta 182 (2018) 558.
[51] J.D. Weatherston, R.K.O. Seguban, D. Hunt, H.J. Wu, ACS Sensors 3 (2018) 852.
[52] J.D. Weatherston, S. Yuan, C.V. Mashuga, H.-J. Wu, Sensors Actuators B Chem. 297 (2019) 126765.
[53] A. Kohut, G. Galbács, Z. Márton, Z. Geretovszky, Plasma Sources Sci. Technol. 26 (2017) 045001.
[54] A. Kohut, L.P. Villy, T. Ajtai, Z. Geretovszky, G. Galbács, J. Aerosol Sci. 118 (2018) 59.
[55] M. Valenti, A. Venugopal, D. Tordera, M.P. Jonsson, G. Biskos, A. Schmidt-Ott, W.A. Smith, ACS Photonics 4 (2017) 1146.
[56] S. He, J. Chua, E.K.M. Tan, J.C.Y. Kah, RSC Adv. 7 (2017) 16264.
[57] P.M. Fierro-Mercado, S.P. Hernández-Rivera, Int. J. Spectrosc. 2012 (2012).
[58] R. Que, M. Shao, S. Zhuo, C. Wen, S. Wang, S.-T. Lee, Adv. Funct. Mater. 21 (2011) 3337.